3.5.4 ICRS Centre

Introduction

The IAU has charged the IERS with the responsibility of monitoring the International Celestial Reference System (ICRS), maintaining its current realization, the International Celestial Reference Frame (ICRF), and maintaining and improving the links with other celestial reference frames. Starting in 2001, these activities have been run jointly by the ICRS Centre (Observatoire de Paris and US Naval Observatory) of the IERS and the International VLBI Service for Geodesy and Astrometry (IVS), in coordination with the IAU. The present report was jointly prepared by the Paris Observatory and US Naval Observatory components of the ICRS Centre. The ICRS Centre web site <http://hpiers.obspm.fr/icrs-pc> provides information on the characterization and construction of the ICRF (radio source nomenclature, physical characteristics of radio sources, astrometric behavior of a set of sources, radio source structure). This information is also available by anonymous ftp (<hpiers.obspm.fr/icrs-pc>), and on request to the ICRS Centre (icrspc@hpopa.obspm.fr).

Maintenance and extension of the ICRF and investigation of future realizations of the ICRS

The International Celestial Reference System (ICRS), adopted by the International Astronomical Union (IAU) in 1997, forms the underlying basis for all astrometry by defining the reference directions of a quasi-inertial celestial coordinate system that are fixed with respect to the most distant objects in the universe. Since 1 January 1998, the ICRS has been realized by the International Celestial Reference Frame (ICRF), which is based on the radio wavelength astrometric positions of compact extragalactic objects determined by the technique of very long baseline interferometry (VLBI).

At the XXVII General Assembly of the IAU held in Rio de Janeiro, Brazil, a second realization of the International Celestial Reference Frame (ICRF2; Fey, Gordon and Jacobs 2009; Fey et al. 2015) was adopted as the fundamental celestial reference frame as of 1 January 2010. ICRF2 is again based on the radio wavelength astrometric positions of compact extragalactic objects determined by the technique of VLBI. Significant developments and improvements in geodetic/astrometric VLBI observing and analysis have been made since the initial generation of the ICRF, hereafter ICRF1. Sensitivity of VLBI observing systems to weaker sources and overall data quality have improved significantly due to advances in VLBI receiver and recording systems and due to better observing strategies coordinated by the International VLBI Service for Geodesy and Astrometry (IVS). The use of newer and more modern radio telescopes, such as the 10-station Very Long Baseline Array (VLBA) of the National Radio Astronomy Observa-

tory (NRAO) has also greatly improved the sensitivity and quality of recent data. Further, enhanced geophysical modeling and computers with faster processors have allowed significant improvements in data analysis techniques and astrometric position estimation.

ICRF2 contains precise positions of 3414 compact extragalactic sources, more than five times the number as in ICRF1. The ICRF2 has a noise floor of approximately 40 micro-arcseconds, some 5–6 times better than ICRF1, and an axis stability of approximately 10 micro-arcseconds, nearly twice as stable as ICRF1. Alignment of ICRF2 with the ICRS was made using 138 stable sources common to both ICRF2 and ICRF1. Maintenance of ICRF2 is made using a set of 295 “defining” sources selected on the basis of positional stability and the lack of extensive intrinsic source structure. The stability of these 295 defining sources and their more uniform sky distribution addresses the two largest weaknesses of ICRF1.

At the IAU General Assembly in Beijing in August 2012, ICRS Centre personnel organized an effort to establish an IAU Working Group on ICRF3. The effort was well received by the IAU. A steering committee was established which met in Beijing and subsequently in October 2012 in Bordeaux. The steering committee wrote a charter for the working group, established working group membership, and selected a working group chair. The IAU subsequently accepted all these and formally established the working group.

The ICRF3 Working Group has since pursued new observations that filled gaps and improved weaknesses of ICRF2, including additional observing at higher radio frequencies, e.g., K-band (24 GHz), Ka-band (32 GHz), and Q-band (43 GHz), where contributions to source position uncertainties from intrinsic source structure and from the Earth’s ionosphere will be less than that at the radio frequencies currently used for astrometric/geodetic VLBI, and second epoch observations of VLBA Calibrator Survey sources (Gordon et al. 2016). The ICRF3 Working Group presented a progress report to the IAU General Assembly in 2015 and continued to pursue the completion of ICRF3 in 2018.

In the coming decades, there will be significant advances in the area of space-based optical astrometry. Missions such as the European Space Agency’s (ESA) Gaia mission, which launched 19 December 2013, are expected to achieve astrometric positional accuracies equal to or better than the accuracies presently obtained by ground-based radio interferometric measurements. Whether future versions of the ICRF exist at multiple wavelengths or are transitioned from the radio to the optical depends at least partially upon the relative astrometric accuracy of future radio- and optical-based reference frames.

Analysis of recent VLBI catalogs

Data sets

Six catalogs were submitted respectively in 2015 by the Italian Space Agency (ASI; asi2015a), Geoscience Australia (aus2015c; aus2016a/b), the Federal Agency for Cartography and Geodesy (BKG Leipzig) and Institute of Geodesy and Geoinformation of the University of Bonn (IGGB) (bkg2015a), and the US Naval Observatory (usn2015b). All these catalogs provide right ascension (α) and declination (δ) of extragalactic radio sources, as well as their respective uncertainties, the correlation coefficient between α and δ and the number of sessions and delays. Note that bkg2014a and usn2015a were produced with the same geodetic VLBI analysis software package SOLVE developed at NASA GSFC. Solutions aus2015c and aus2016a/b were produced with OCCAM.

Table 1 displays the total number of sources of each catalog, as well as the number of ICRF2 sources (out of 3414) and ICRF2 defining sources (out of 295). Some catalogs do not provide values for some defining sources, likely because they do not process some sessions that were present in the session list processed to generate the ICRF2 catalog. We recommend that the analysis centers pay attention to their session list in order to get values for all 295 ICRF2 defining sources. As well, none of the catalogs provide values for all 3414 ICRF2 sources (as was previously noted in the 2014 Annual Report).

The median error reported in Table 1 reveals an error in declination larger than in right ascension by a factor of ~1.5. The error is substantially smaller for SOLVE solutions compared to OCCAM, except the solution asi2015a whose smaller error likely originates in the fact that the solution considered a relatively small number of well observed sources with low positional standard error.

Frame orientation

We evaluate the consistency of the submitted catalogs with the ICRF2 by modeling the coordinate difference (in the sense catalog minus ICRF2) by a 6-parameter transformation as used at the IERS ICRS Center in previous comparisons:

Table 1: Number of sources by categories and median error. Unit is µas. Values for right ascension are corrected from the cosine of the declination.

	No. Sources			Median Error	
	Total	ICRF2	Def	RA	Dec
asi2015a	944	936	294	37.3	41.2
aus2015c	3683	3235	295	1276.5	1780.0
aus2016a	3900	3282	295	526.5	728.0
aus2016b	3917	3288	295	520.5	700.0
bkg2015a	3398	3112	294	284.6	430.2
usn2015b	4110	3316	287	231.0	333.7

$$A1 \tan\delta \cos\alpha + A2 \text{ tg } \delta \sin\alpha - A3 + DA\,(\delta-\delta_0) = \Delta\alpha,$$
$$-A1 \sin\alpha + A2 \cos\alpha + DD\,(\delta-\delta_0) + BD = \Delta\delta,$$

where A1, A2, A3 are rotation angles around the X, Y, and Z axes of the celestial reference frame, respectively, DA and DD represent linear variations with the declination (which origin δ_0 can be arbitrarily chosen but was set to zero in this study), BD is a bias in declination, and $\Delta\alpha$ and $\Delta\delta$ are coordinate differences between the studied and the ICRF2 catalogs. The 6 parameters were fitted by weighted least squares to the coordinate difference of the defining sources (upper part of Table 2) and ICRF2 sources (lower part of Table 2) found in the catalog. The standard deviation of the offsets to ICRF2 after removal of the systematics of Table 2 is reported in Table 3 together with the median offset.

The three Australian solutions show non statistically significant rotations and deformations with respect to the ICRF2. Significant misorientation around A2 larger than 10 mas (4 sigmas) are found

Table 2: Rotation parameters with respect to ICRF2. A1, A2, A3 and BD are in µas. DA and DD are in µas per degree.

	A1	A2	A3	DA	DD	BD
Defining sources						
asi2015a	-2.3	16.4	-13.1	0.2	1.0	-68.5
+-	3.6	3.6	3.3	0.1	0.1	3.5
aus2015c	-9.5	2.9	2.2	-0.0	0.2	3.0
+-	3.0	3.0	2.9	0.1	0.1	2.9
aus2016a	-6.3	2.1	4.5	-0.0	-0.0	4.2
+-	3.4	3.4	3.2	0.1	0.1	3.3
aus2016b	-4.6	-0.3	4.8	0.1	-0.1	4.8
+-	3.0	3.0	2.8	0.1	0.1	2.9
bkg2015a	-9.3	12.3	-9.1	0.2	1.1	-64.2
+-	4.3	4.3	3.8	0.1	0.1	4.2
usn2015b	-7.2	16.3	-0.4	0.2	0.9	-53.2
+-	3.8	3.8	3.3	0.1	0.1	3.6
All common sources						
asi2015a	2.5	18.9	-14.1	0.2	1.2	-70.6
+-	2.8	2.8	2.6	0.1	0.1	2.6
aus2015c	-4.4	2.2	-3.9	-0.1	0.3	0.6
+-	1.2	1.2	1.2	0.0	0.0	1.1
aus2016a	-1.8	1.3	-3.3	-0.2	0.1	1.2
+-	1.2	1.2	1.1	0.0	0.0	1.1
aus2016b	-0.5	0.1	-0.2	-0.0	0.0	0.2
+-	0.2	0.2	0.2	0.0	0.0	0.2
bkg2015a	-4.1	14.7	-10.9	0.1	1.3	-66.2
+-	1.5	1.5	1.4	0.1	0.0	1.4
usn2015b	-2.8	20.4	-7.1	-0.0	1.1	-57.2
+-	1.4	1.4	1.3	0.0	0.0	1.3

Table 3: Statistics after removal of systematics given in Tables 2. Unit is μas. Values for right ascension are corrected from the cosine of the declination.

	Standard Deviation				Median Offset			
	Defining		All		Defining		All	
	RA	Dec	RA	Dec	RA	Dec	RA	Dec
asi2015a	55.5	64.8	141.6	323.6	49.7	61.4	50.3	61.4
aus2015c	53.6	48.5	128.4	161.2	247.5	488.0	269.2	450.6
aus2016a	51.9	43.9	139.4	173.0	247.9	442.3	261.7	438.3
aus2016b	7.8	5.5	33.2	39.3	242.4	455.6	246.6	414.8
bkg2015a	53.7	61.8	362.7	364.1	118.1	222.5	121.5	209.2
usn2015b	60.0	65.4	565.1	863.2	126.5	238.4	134.7	230.4

for other catalogs. The largest deviation from ICRF2 axes is observed for the bias in declination. Values of BD are significantly larger than the ICRF2 axis stability of 10 mas measured at the time of the ICRF2 release in 2009 (Fey et al. 2015). This fact may indicate some systematics in source declinations with respect to solutions of the previous years and may have to be considered in parallel to the zonal declination error raised in the 2012–2015 ICRF3 WG documentation (e.g., Jacobs et al. 2014). Note that this particular point should be addressed rigorously in the framework of the 2016–2018 ICRF3 WG.

Zonal errors

Figure 1 displays the offset to ICRF2 (in the sense catalog minus ICRF2) averaged over declination bins of 5 degrees. All solutions but Australian ones exhibit declination errors offset to the negative part of the plot, that may reflect the large values of BD found in the coordinate difference to ICRF2. However, no pronounced dependence in declination shows up for any solution.

Standard error and noise

Figure 2 illustrates how the overall formal error, defined as the square root of $\sigma_{\alpha\cos\delta}^2+\sigma_\delta^2+c\sigma_{\alpha\cos\delta}\sigma_{\alpha\delta}$ where σ is the formal error listed in the catalogs and c is the correlation coefficient between estimates of α and δ as provided in the catalogs, varies with the number N of observations. The circled dots represent defining sources. The figure for aus2016b clearly shows that the defining sources have underestimated formal errors likely due to an overconstrained solution. (As stated in the technical document delivered with the catalog, a strong no-net rotation condition imposed to these sources. Similar fact was pointed for solution aus2015a in the IERS Annual Report 2014.) The formal error of the same sources in solution aus2015c and aus2016a, in which the no-net rotation condition is less severe, appears to be at a level comparable to other sources.

Figure 2 also shows how the error on delays is propagated to the estimated source coordinates. For white noise measurements,

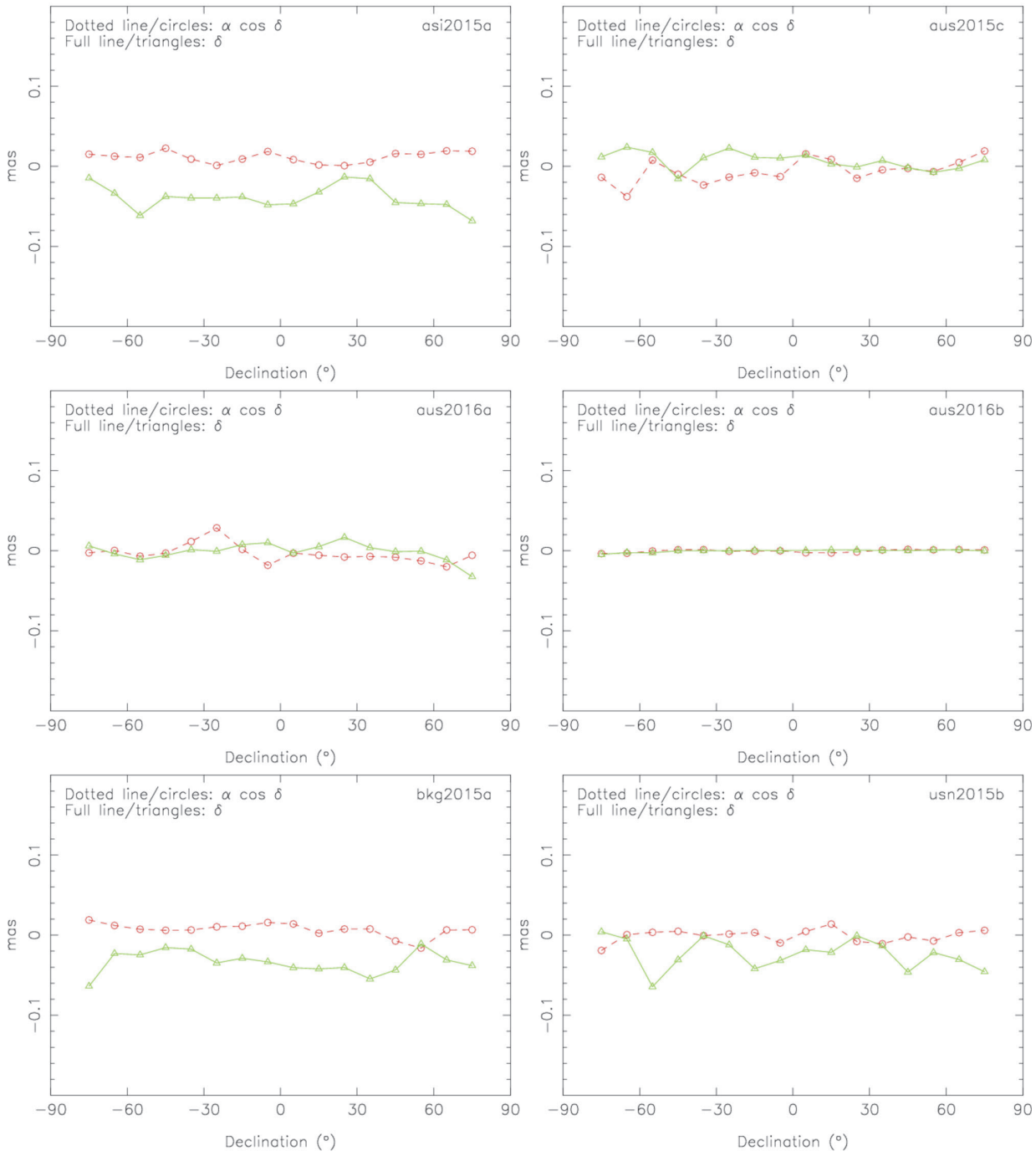

Fig. 1: Offset to ICRF2 for right ascension (dotted line with circles) and declination (full line with triangles) by bins of declination of 5 degrees.

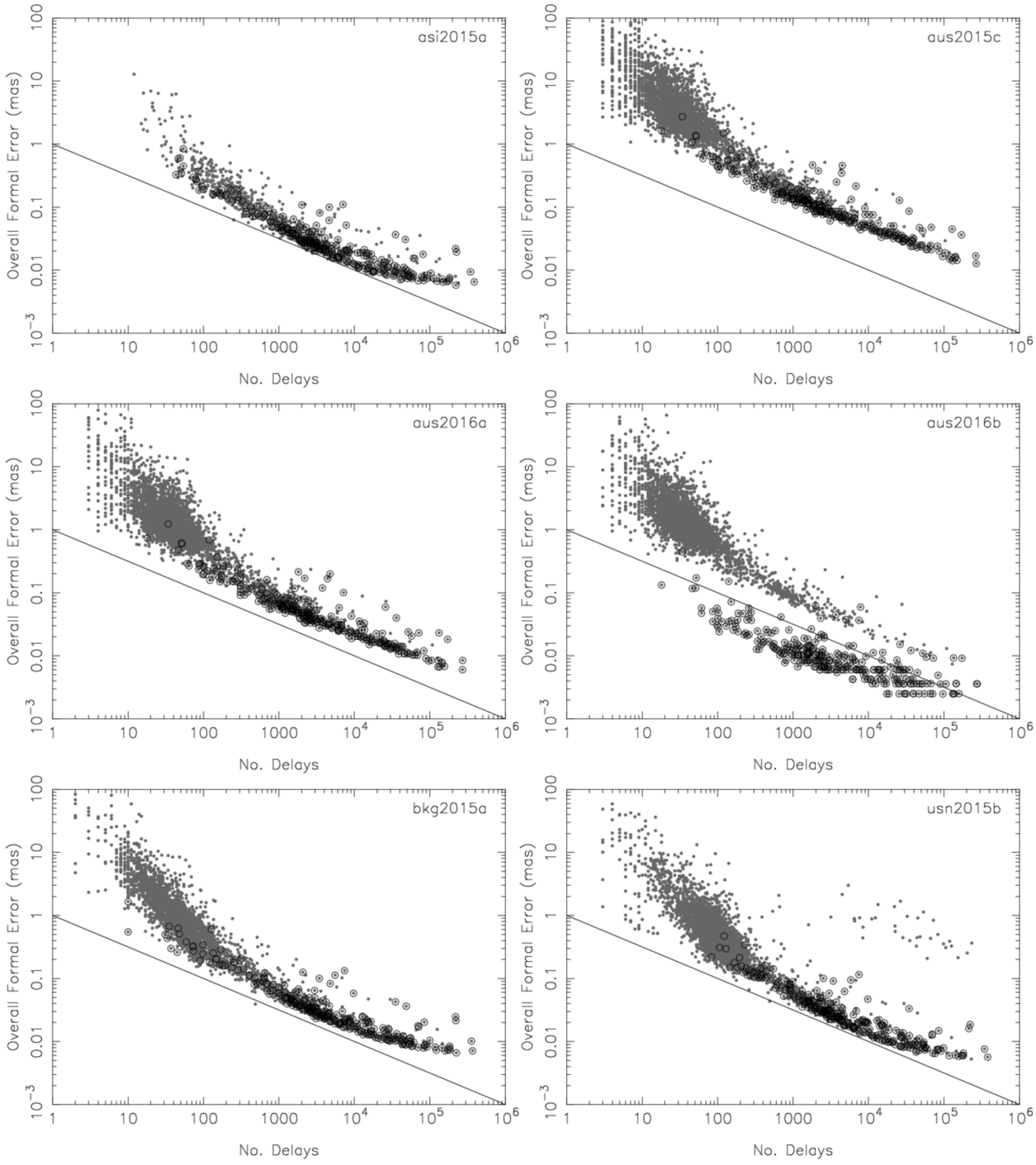

Fig. 2: Overall formal error as a function of the number of observations. The circled dots represent defining sources. The solid line indicates a decrease as $N^{-1/2}$ where N is the number of delays.

the formal error on source coordinates is expected to decrease as $N^{-0.5}$. The figure reveals that this regime exists for N between ~100 and ~10000. For N lower than a hundred observations (e.g., VCS sources or sources observed in only one session) the formal error varies as N^{-1}. Beyond 10000 observations, the formal error generally tends towards a limit lower than ~10 mas. Such a deviation is visible for all catalogs but the Australian ones for which the formal error seems to continue to decrease more closely (but not exactly) to $N^{-0.5}$. The deviation for large N observed for all other catalogs is likely the signature of non-Gaussian correlated errors: as N increases, thermal baseline-dependent error tends to zero and the station-dependent error arising from time- and space-correlated parameters becomes dominant (see, e.g., Gipson 2006 or Romero-Wolf et al. 2012; see also Lambert 2014).

A last test was performed to assess the consistency between the formal errors and the offset to ICRF2. This test was motivated by the consideration that, although the ICRF2 is not the "truth", it nevertheless provides accurate values of well-observed sources. As a consequence, for most of the sources, the addition of new observations after 2009 should not perturb significantly the estimated position but only improve the formal error. Figure 3 displays the scatter around the ICRF2 position computed for bins of increasing formal error. For a white noise, one should get values close to the first diagonal (i.e., the formal error fully explains the offset to ICRF2). For formal errors lower than 0.1 mas, one sees that the scatter is over the diagonal, indicating a possible underestimation of the formal errors. To quantify this scale factor, one can estimate it together with an error floor so that a realistic error Er (i.e., that explains the observed offset to ICRF2) is given by

$$Er = ((E\ s)^2 + f^2)^{-0.5}$$

where E is the error, s a scale factor and f a noise floor. Values of s and f estimated over sources whose offset to ICRF2 is smaller than 1 mas are reported in Table 4. Uncertainties are ~0.01 mas on s and ~0.01 on f. SOLVE solutions tend to have scale factors larger than unity while OCCAM catalogs have scale factors smaller than 1. Note that the noise floor does not represent the catalog internal error since one considers the offset to ICRF2: the quantity f therefore contains the internal noise of the ICRF2. The global noise lies between 0.05 and 0.12 mas. If one assumes 0.04 mas for the ICRF2 internal noise (Fey et al. 2015), it means that the analyzed catalog internal noises are larger by a factor between 1 and 3.

Conclusions and recommendations

The above results lead to some recommendations for analysis centers who plan new submissions in the future. First, it is recommended to include all ICRF2 sessions in the processed session list, in order to get values of, at least, all 3414 ICRF2 sources. Second,

Table 4: Noise floor and scale factor estimated for sources with offset lower than 1 mas. Unit is µas. Values for right ascension are corrected from the cosine of the declination.

	-- Floor --		-- Scale --	
	RA	Dec	RA	Dec
asi2015a	42.7	55.6	3.65	3.07
aus2015c	46.7	40.5	0.60	0.60
aus2016a	48.3	43.6	1.14	1.11
aus2016b	7.3	7.7	1.17	1.12
bkg2015a	50.7	66.4	1.34	1.18
usn2015b	57.6	71.2	1.64	1.54

analysis centers should focus on understanding several points: (i) the significant systematics in orientation (~0.05 mas) showing up in Table 2, (ii) the zonal errors appearing in Fig. 1 for some solutions, and (iii) the non-Gaussian errors dominating for large number of observations raised by Fig. 3. About the latter item, one should understand particularly why the OCCAM solutions decreases differently than SOLVE catalogs for larger numbers of delays. In the future, the correction of this defect should be achieved by better modeling and parameterization of clock and troposphere correlated errors, consistently in all VLBI analysis software.

The Large Quasar Astrometric Catalog (LQAC) and related studies

The Large Quasar Astrometric Catalog

The ICRS Center is in charge of the LQAC (Large Quasar Astrometric Catalog), a whole sky compilation of information on known QSOs, as well as of its regular up-dates. The second release of the LQAC, (LQAC-2) (Souchay et al., 2012) was published as a CDS catalog. It contained 187 504 quasars. A third release, the LQAC-3, was published in 2015 (Souchay et al., 2015). It contains 321 957 objects, which represent a 71.7% increase with respect to the LQAC-2.

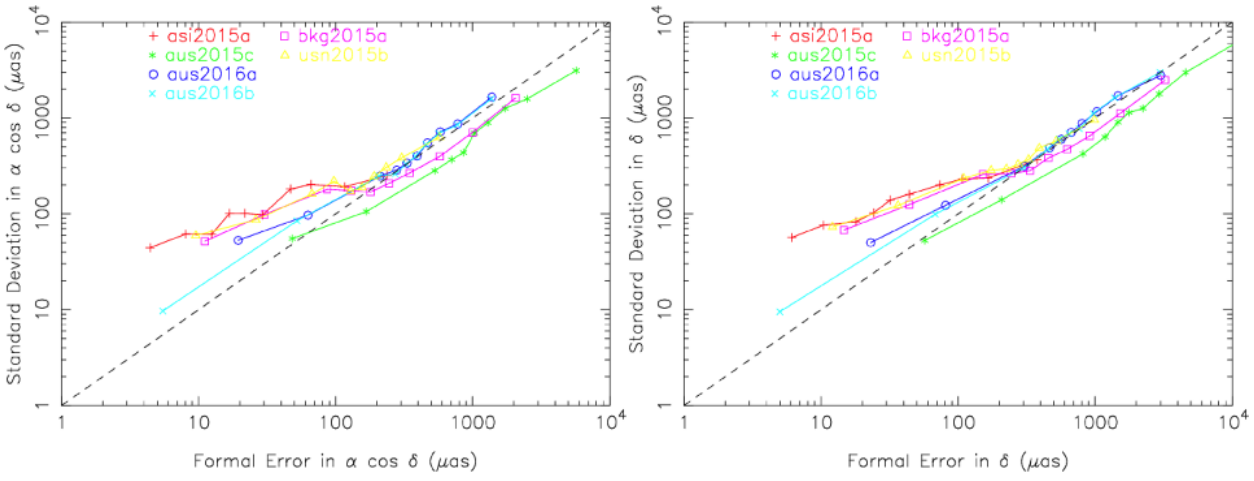

Fig. 3: Scatter of the offset to ICRF2 versus the formal error.

Basically, the LQAC delivers complete information (when available) as a set of optical magnitudes and radio fluxes, the redshift, original and consolidated equatorial coordinates, together with re-calculated absolute magnitudes and morphological indexes (see IERS Annual Report, 2010, 2012).

Related studies

The construction of the third edition of the Large Astrometric Quasar Catalog – LQAC3 (Souchay et al., 2015) enabled the in-depth study of the large, coherent sample of quasars represented by the SDSS-III DR10Q (Pâris et al., 2014). Its astrometric properties could be independently checked out from the 190,184 new SDSS quasars, as compared to the ones determined in previous editions of the LQAC (Souchay et al., 2012). It is likewise concerning the PSF-morphology properties, in this case specially interesting because the new quasars in the DR10Q come from the Baryon Oscillation Spectroscopic Survey – SDSS-III: BOSS (Ross et al., 2013), with redshift in the range z = [2.2,3.5], which corresponds to a very relevant stretch of the quasar luminosity function, when the quasar number density and luminosity were maximal.

To render the LQAC3 astrometric positions compliant to the ICRF2, the steps presented in the Large Quasar Reference Frame (LQRF and LQRF2) (Andrei et al. 2009; Souchay et al. 2012) were followed. For 123,448 SDSS sources the LQAC2 positions are recognized in the LQAC3 (1” matching), meaning just minor corrections on the prior SDSS releases. On average the difference of positions is very small (–0.1 mas in R.A. and 4.2 mas in DEC.) but the mean distance between corresponding positions is non-negligible (61.2 mas). As for the quasars not belonging in the LQAC2, the local corrections and magnitude corrections were found negligible. The global analysis confirms the previous findings in that the director cosines around the ICRF equinox and contra-equinox axis are small. However, the director cosines representing corrections to the right ascension and declination origins are significant. Their values are respectively –9.1 (± 1.8) mas, and 4.1 (± 2.0) mas. Also as expected the systematic corrections for zonal warps are small (–0.9 mas in R.A. and 1.0mas in DEC.), nevertheless the resulting average displacement is of 54.5 (± 12.8) mas. The combination of corrections for the global rotation and for the systematic local deviations is effective and the mean distance between the ICRF and LQRF-type positions is slashed to 21.6 (± 13.4) mas. In conclusion, these positions or a conveniently chosen subset can provide a good independent comparison for the alignment to the ICRF for the Gaia first data release.

The aspects of morphology and variability were crucial for selecting the quasars to form the ICRF (Ma et al., 2009), based on radio VLBI observations. Also on the optical band these two aspects are increasingly addressed in programs of high astrometric precision.

For the Gaia mission, we can use the morphological indexes included in the Gaia Initial QSO Catalog – GIQC (Andrei et al., 2012). In radio waves bright spots are commonly formed where shocks traveling up the jets exchange energy with the external medium (Begelman et al., 1984), and are often taken as the radio centroid. In contrast to this, light emitted in (and around) the optical window originates mostly from the very central part of the quasar, either by thermic processes in the accretion disk, or relativistic processes at the bases of the jets. But light also originates from the host galaxy and, though comparatively less, from line emission processes and as a consequence of the heating of more distant surrounding dust. Thus much effort has been put in disentangling the central source and the galaxy isophotes by modeling. This was indeed proposed in the formulation of the GIQC and is implemented for all quasars observations in the Gaia mission (Ducourant et al., 2014). To characterize the extent of the influence of the host on the compound image, which is crucial for astrometric purposes, the analysis of a single PSF fitting can be made.

For the LQAC3 the approach of analyzing the PSF of the quasar image in comparison with the local mean PSF of stars of similar magnitude is the same adopted in the former versions of this compilation. The elements of comparison are the parameters SHARP, SROUND, and GROUND, determined by IRAF's DAOFIND on the Johnston B, R, and I digitized plates of the DSS. The morphological indexes of each quasar are given by the same formula as (Andrei et al., 2008):

$$M_{PC} = | PQ - Ps | / \sigma$$

where M_{PC} is the morphological index of quasar Q for the PSF parameter P in the color C, given in comparison to the mean value from the stars Ps, and normalized by the stellar standard deviation σ.

As we have noted previously, while a great majority of quasars are stellar-like in appearance, a significant proportion of quasars display a PSF that is apparently disturbed by an otherwise not-easily-detectable host. Furthermore, the more conspicuous the host, the more we observe a shift from B to I. For every quasar at least one morphological index was obtained (that is, at least one good image exists). For 59% of the entries we got all the 9 morphological indexes. The direct comparison with the same morphological indexes for the stars provided a sanity test verifying null averages and standard deviations of about 0.9 for SHARP, 0.7 for SROUND, and 0.8 for GROUND, slightly smaller at I than B, but without statistically significant evolution over magnitude from R = 9 to 22. DAOFIND has been largely and successfully used, for instance, in the detection of clusters (Bastian et al., 2011). The way to circumvent its performance degradation in low illumination

regimes is to use a “logical training process” (Mähönen and Hakala, 1995), which was done in the present case by using the nearby, similar magnitude stars.

The main features of the morphological indexes for the new sources in the LQAC3 are the same as in the former versions. However the populations from which the sources are drawn present differences, as described above. The quasar luminosity function is such that increasing redshift is counterbalanced by increasing luminosity, with the result that the dimming of apparent magnitudes is much reduced. As the energy is fed back from the active nuclei to the host galaxy, the later often presents as a massive elliptical with significant quantities of dust and high rate of star formation, compatible with both infrared and UV emission. But direct imaging is unlikely to be feasible due to the cosmological dimming in surface brightness. In order to maximize the certainty of the morphological indexes for the new, more distant sources included in the LQAC3, three conservative steps were taken. The source count was calculated and then convolved with the one from Mähönen and Hakala (1995) that downsizes the indexes. The analysis was restricted to only sources brighter than R = 19 magnitude. The DSS images matches were concurrently searched for in the PPMXL catalogue, limiting the matches to those close in angular distance, in magnitude, and of negligible proper motion.

Comparing the PPMXL- and non-PPMXL-found quasars, the correlation over all plates and morphological indexes is 99.9%, thus clearly implying that the images on the DSS plates were found correctly and that the training of the morphological indexes renders magnitude effects unimportant. The end-result is that mostly stellar-like close-to-zero values are found, as before, increasingly from B to I. Much less obviously, within each color, the averages of the morphological remain nearly constant on redshift, which would favor a scenario of coevolution of galaxies and supermassive black holes (Heckman and Best, 2014).

Monitoring of QSOs

During the year 2015 the magnitude monitoring of QSO for the link between reference systems (ICRF/GCRF) was achieved with the help of small and medium size optical telescopes. The TAROT program (<http://tarot.obs-hp.fr/>) was the first effort. It has produced series of observations with long temporal baselines and relatively high frequencies (one observation every two days over five years). Taris et al. (2016) describes the results through 2016. As shown in the paper, some sources display clear periodic variations in brightness. For the 14 targeted QSO’s observed with these instruments, we determined periods, with confidence levels above 90% in all cases. Some of the periods found were not previously known. For the other targets, we did a comparative study

of the periods previously studied by other authors and confirmed their values. All the periods given by the two methods are in good agreement with each other, with differences less than 7.9% for the worst case. Finally we also presented the structure functions for our two sets of objects (BL Lac and Seyfert galaxies).

A second program, in close collaboration with G. Damljanovic from Belgrade Observatory, was achieved using three 60cm optical telescopes. They are located at Vidojevica (<http://vidojevica.aob.rs/index.php?option=comcontent&view=article&id=22&Itemid=29>), Rozhen (<http://www.nao-rozhen.org/telescopes/fr16_en.html>) and Belogradchik (<http://www.astro.bas.bg/~aobel/equipment.html>) observatories. The LFOA 1.5m telescope (<https://astro.univie.ac.at/foa/teleskope-instrumentation/15m-teleskop/>) and the TJO telescope 0.8m (<http://www.oadm.cat/en/content/45/tjo.htm>) were also included in this program devoted to photometric monitoring of targets other than those mentioned previously. The goal of this program is to compare the brightnesses of the QSO's with the G magnitudes that will be provided by the first release of the Gaia catalogue (DR1 to be published in 2016).

A third program began in 2015 in collaboration with Z. Malkin from Pulkovo Observatory. It is devoted to the observation, with the TJO, of targets coming from the OCARS catalogue (<http://www.gao.spb.ru/english/as/ac_vlbi/>). Due to the very large number of targets (>5000), this program will be completed during the year 2017. The goal is to observe a set of targets that have been observed with the radio VLBI techniques but which are not very well known from the optical point of view. In this way, we can put limitations on the magnitudes/variability of the targets and then, extend the lists of target suitable for the link between the reference systems.

The programs mentioned are all very time consuming due to the large number of targets that must be monitored. Moreover these programs are done within the framework of competitive international calls for proposal. This last point could be an issue when the total observation time requested is important. To avoid these constraints, the SYRTE department of Paris Observatory plans to build a robotic telescope dedicated to the photometric monitoring of QSO's. The first part of this project began in 2015 by the choice of a site with a good atmosphere, characterized by its good seeing. During the 1970s the French government wanted to build a four meter telescope that became later the 3.6m Canada France Hawaii Telescope (CFHT) on top of Mauna Kea volcano. For this purpose, sites were selected in Europe with respect to their high quality in terms of astronomical seeing. We choose one of them, Saint-Véran (alt. 3000m), in the French Alps, near the Italian border, for implementing a site seeing monitoring campaign (<http://stveran.obspm.fr/index.php?page=statistiques>). The goal

of this campaign is to show, with modern instruments, that the site seeing is effectively the expected one.

Quasar Source Structure Databases

Radio Reference Frame Image Database

The Radio Reference Frame Image Database (RRFID) is a web-accessible database of radio frequency images of ICRF sources. The RRFID currently contains 7279 VLBA images of 782 sources at radio frequencies of 2.3 GHz and 8.4 GHz. Additionally, the RRFID contains 1867 images of 285 sources at frequencies of 24 GHz and 43 GHz. Imaging of additional radio sources has been temporarily suspended due to lack of available resources. The RRFID can be accessed from the Analysis Center web page or directly at <http://rorf.usno.navy.mil/rrfid.shtml>.

Bordeaux VLBI Image Database

The Bordeaux VLBI Image Database (BVID) is a web-accessible database of radio frequency images of ICRF sources. The BVID currently contains 5719 VLBA images of 1273 sources mostly at radio frequencies of 2.3 GHz and 8.4 GHz, but includes images for some sources at 24 GHz and 42 Ghz. Corresponding structure correction and visibility maps are also available. The BVID can be accessed from the Analysis Center web page or directly at <http://www.obs.u-bordeaux1.fr/BVID/>.

Link Between Optical and Radio Reference Frames

Work continued to assess the potential magnitude and explanation for offsets in position between extra-galactic reference frame objects in the optical and in the radio. Analysis of data obtained at CTIO from 1997 to 2004 that used a combination of simultaneous UCAC astrograph and CTIO 0.9m observations in the same bandpass, indicates systematic differences in positions between the optical and radio positions of ICRF2 sources exceeding 100 mas in some cases with suspected general, random offsets of most sources of order single mas (see Zacharias and Zacharias, 2014). If this new and potentially significant source of error holds for alignment sources common to both Gaia and the ICRF, then the optical/radio system alignment error of a significant fraction of a milliarcsecond could result. Results of the reference frame link work were presented at the December 2014 Extra-Galactic Science with Gaia (EGSG) meeting, held at Observatoire de Paris-Meudon and the July 2015 Gaia for AGN and Extragalactic Science (GAGNES) meeting at Paris Observatory. Additional analysis of this issue, along with new optical and radio observations have been conducted in 2015, and the results communicated to the Gaia team and ICRF3 working group.

During 2015, USNO concluded a decade-long monitoring program of 12 selected ICRF sources with optical counterparts using the NOFS Strand 1.55 m astrometric telescope. Relative positions with respect to selected reference stars in the same field of view were derived in a fashion similar to the trigonometric

parallax program at that telescope. Changes in optical position of these extragalactic targets as a function of observing epoch were fitted with a parallax and proper motion contribution to remove the average reflex motion of the reference stars in each field.

For at least one source, ICRF 0754+100, a significant change in optical position as a function of brightness is found. A possible explanation is an astrophysical position offset of the bright AGN core with respect to the surrounding light of the host galaxy. The average light of the host galaxy is assumed to be constant over the 10 year period while the core of this ICRF defining BL-Lac object varies by about 2 magnitudes over the period of our observations causing the combined center of light to shift. Details will be published in an upcoming paper (Harris et al. 2016).

Optical Astrometric Catalogs

In June 2015 the three-year observing program with the USNO Robotic Astrometric Telescope (URAT) concluded at its northern hemisphere site, the Naval Observatory Flagstaff Station (NOFS) (see Figure 4). The URAT1 catalog, covering the Northern Hemisphere and red magnitudes 3–18, was published in February 2015 (Zacharias, Finch, Subasavage et al., 2015) (see also IERS Annual Report 2014), which gives accurate positions of over 200 million objects based on the first two years of observing at NOFS. These data were supplemented by preliminary proper motions using 2MASS as early epoch.

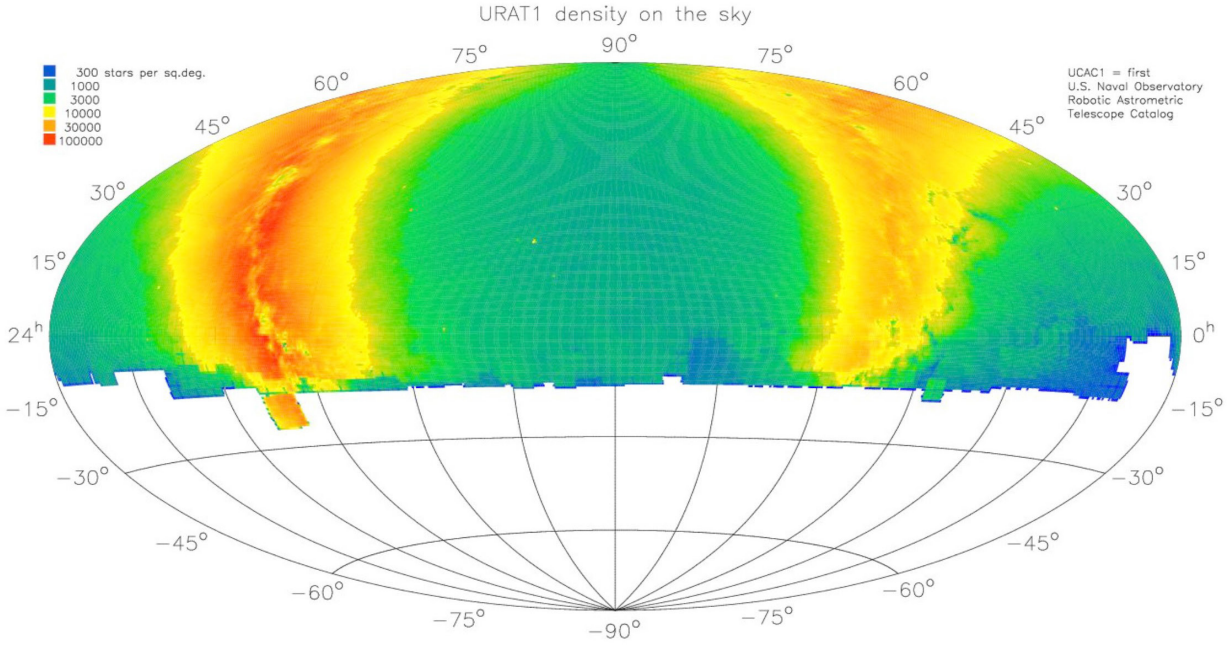

Fig. 4: URAT sky overage as of late 2014. The 2015 URAT1 release consists of over 228 million stars covering the sky north of approximately –15 deg DEC. URAT1 includes observations from April 2012 to June 2014, along with extensive validation using a variety of sources.

An internal catalog (URAT2) covering the full three-year northern program was constructed providing access to mean positions as well as individual observations. The optical positions have been put on the ICRF by using UCAC4 as reference star catalog. These data were used to look at optical counterparts of radio reference frame sources. Over 2100 sources in common with the 2014 version of the Radio Fundamental Catalog (RFC, Petrov, <http://astrogeo.org/rfc/>) were found in the URAT data. Position differences (separation on the sky in mas) divided by the combined, formal errors of the radio and optical position (also in mas) for each source were calculated (unit is standard error or sigma). Figure 5 shows a plot of these normalized position differences as a function of redshift z after excluding sources with 9 or more sigma position differences (to eliminate grossly wrong data) and binning to better show systematic trends. Nearby sources clearly show a larger position difference than cosmologically more distant sources indicating a contribution likely from real astrophysical optical to radio position center offsets. These results and other ground-based catalog data related to radio-optical sources were presented at the 2015 GAGNES meeting in Paris.

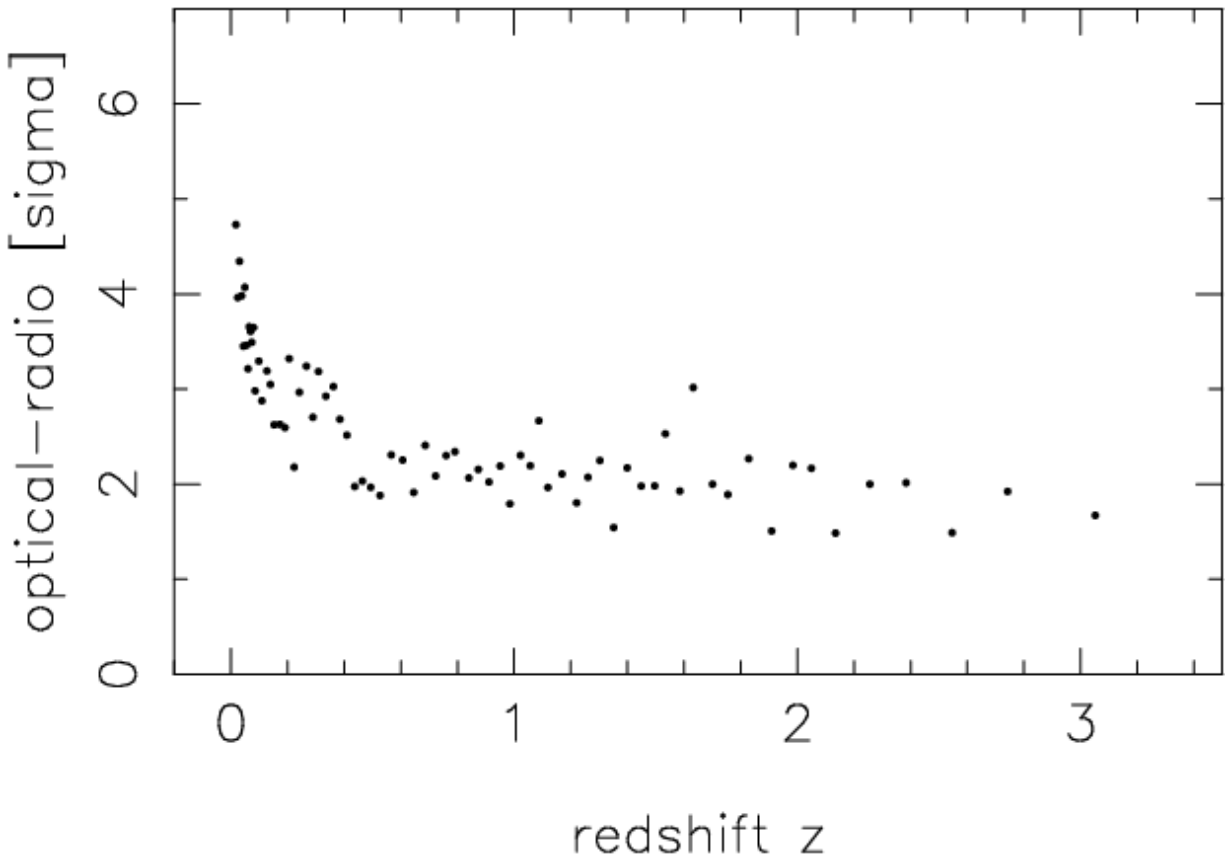

Fig. 5: Normalized position differences between URAT1 and RFC sources (AGN) as a function of redshift. Obvious mismatches (sigma ≥ 9) have been excluded.

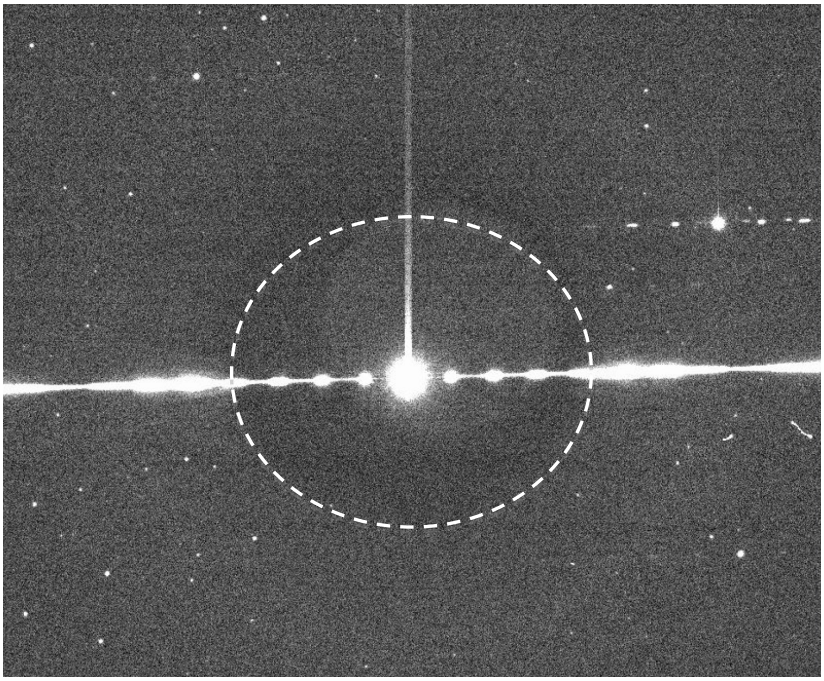

Fig. 6: URAT five second exposure of Sirius (v = –1.46) with grating in place showing approximate extent of ND filter.

In October 2015 the URAT astrograph began a southern hemisphere survey after successful relocation to the Cerro Tololo Interamerican Observatory (CTIO). Because of the upcoming 1st Gaia data release, this southern survey is concentrating on the very bright stars. For this purpose, a new neutral density spot has been added to the camera dewar window that is large enough to include the 1st order grating images.

Figure 6 shows a single, five-second exposure taken with the URAT astrograph of Sirius, the brightest star in the sky. The central image is overexposed beyond recovery for a good astrometric position. However, the flux of the first order grating images is well below saturation. The extent of the neutral density spot can be inferred from the grating images. Further out images suddenly become about five magnitudes brighter once outside the spot. This observing program will provide accurate positions on the ICRF of such bright stars at current epochs to improve the proper motions when combined with Hipparcos data until being superseded in future years when Gaia data for these stars may become available.

Simultaneously, the USNO Bright-Star Astrometric Database (UBAD) program will observe the brightest stars in the Northern Hemisphere. UBAD will utilize a camera similar in some respects to the URAT camera, with an ND-12 spot and will be deployed on the NOFS 1.55m Strand astrometric telescope to survey the entire Northern Hemisphere. Also, as with URAT, UBAD will use

Gaia astrometric data for the reference stars. Both catalog projects will supplement Gaia data at the bright end, and will be on the Gaia system.

Staff

Dorland, Bryan, Director (USNO)
Souchay, Jean, Co-director (OP)
Andrei, Alexandre, Assoc. Astronomer (OP, Obs. Nat. Rio, Brasil)
Arias, E. Felicitas, Assoc. Astronomer (BIPM / OP)
Barache, Christophe, Engineer (OP)
Bouquillon, Sébastien, Astronomer (OP)
Fey, Alan, Astronomer (USNO)
Lambert, Sébastien, Astronomer (OP)
Taris, François, Engineer (OP)
Titov, Oleg, Astronomer (OP, Geoscience Australia)
Zacharias, Norbert, Astronomer (USNO)

References

Andrei, A. H., Souchay, J., Zacharias, N., et al. 2009, Astronomy & Astrophysics 505, 385

Andrei, A. H., Anton, S., Barache, C., et al. 2012, SF2A-2012: Proceedings of the Annual meeting of the French Society of Astronomy and Astrophysics, 61

Bastian, N., Adamo, A., Gieles, M., et al. 2011, Monthly Notices of the Royal Astronomical Society 417, L6

Begelman, M. C., Blandford, R. D., & Rees, M. J. 1984, Reviews of Modern Physics 56, 255

Bianco, G., et al. 2009, IERS Technical Note 35, 1

Cai, Z., Fan, X., Noterdaeme, P., et al. 2014, Astrophysical Journal 793, id. 139

Ducourant, C., Krone-Martins, A., Galluccio, L., & Teixeira, R. 2014, SF2A-2014: Proceedings of the Annual meeting of the French Society of Astronomy and

Astrophysics, 421

Fey, A. L., Gordon, D., Jacobs, C. S. (eds.) 2009, “The Second Realization of the International Celestial Reference Frame by Very Long Baseline Interferometry”, IERS Technical Note No. 35, Frankfurt am Main

Fey, A. L., Gordon, D., Jacobs, C. S., et al. 2015, Astronomical Journal 150, id. 58

Gordon, D., et al. 2016, Astronomical Journal 151, id. 154

Gipson, J. M. 2006, in: International VLBI Service for Geodesy and Astrometry (IVS) 2006 General Meeting Proceedings, NASA/CP-2006-214140, eds. D. Behrend, & K. D. Baver, 286

H. Harris et al. 2016, Astronomical Journal, in press

Heckman, T. M., & Best, P. N. 2014, Annual Review of Astronomy and Astrophysics 52, 589

Jacobs, C. S., Arias, E. F., Boboltz, D., et al. 2014, in: Proceedings of the Journées 2013 “Systèmes de référence spatio-temporels”: Scientific developments from highly accurate space-time reference systems, Observatoire de Paris, 16–18 September 2013, Edited by Nicole Capitaine, ISBN 978-2-901057-69-7, 51

Lambert, S. 2014, Astronomy & Astrophysics 570, id. 108

Mähönen, P. H., & Hakala, P. J. 1995, Astrophysical Journal 452, L77

Pâris, I., et al. 2014, Astronomy & Astrophysics 563, id. A54

Romero-Wolf, A., Jacobs, C. S., & Ratcliff, J. T. 2012, in: International VLBI Service for Geodesy and Astrometry (IVS) 2012 General Meeting Proceedings, NASA/CP-2012-217504, eds. D. Behrend, & K. D. Baver, 231

Ross, N. P., McGreer, I. D., White, M., et al. 2013, Astrophysical Journal 773, id. 14

Smart, R. L.; Nicastro, L. 2014; Astronomy & Astrophysics 570, id. A87

Souchay, J., Andrei, A. H., Barache, C., et al. 2012, Astronomy & Astrophysics 537, id. A99

Souchay, J., Andrei, A. H., Barache, C., et al. 2015, Astronomy & Astrophysics 583, id. A75

Taris, F. et al. 2016, Astronomy & Astrophysics, in prep.

Wilson, A. S., & Colbert, E. J. M. 1995, Astrophysical Journal 438, 62

Zacharias, N., Finch, C., Subasavage, J., et al. 2015, Astronomical Journal 150, id. 101

Zacharias, N. & Zacharias, M., 2014, Astronomical Journal 147, id. 95

Bryan Dorland, Jean Souchay, Alexandre Andrei,
E. Felicitas Arias, Christophe Barache, Sébastien Bouquillon,
Alan Fey, Sébastien Lambert, François Taris,
Oleg Titov, Norbert Zacharias